Environment International 127 (2019) 848–857

Contents lists available at ScienceDirect

Environment International

journal homepage: www.elsevier.com/locate/envint

The role of soil components in synthetic mixtures during the adsorption and speciation changes of Cr(VI): Conjunction of the modeling approach with spectroscopic and isotopic investigations

Veronika Veselská[a,*], Hana Šillerová[a], Jörg Göttlicher[b], Zuzana Michálková[a], Jamal A. Siddique[a,1], Sylva Číhalová[a,2], Vladislav Chrastný[a], Ralph Steininger[b], Stefan Mangold[b], Michael Komárek[a]

[a] Department of Environmental Geosciences, Faculty of Environmental Sciences, Czech University of Life Sciences Prague, Kamýcká 129, CZ-16500 Prague, Czech Republic
[b] Institute for Photon Science and Synchrotron Radiation, Karlsruhe Institute of Technology, Hermann-von-Helmholtz-Platz 1, DE-76344 Eggenstein-Leopoldshafen, Germany

ARTICLE INFO

Keywords:
Chromate reduction
Soil component mixtures
Adsorption modeling
Cr isotopes
X-ray absorption spectroscopy

ABSTRACT

This study investigates redox transitions associated with the adsorption of Cr(VI) on commonly occurring soil components (silicates, oxides and humic acids) and their synthetic mixtures by coupling the mechanistic surface complexation modeling with spectroscopic and isotopic analyses. The mixtures of soil components were prepared to reflect the composition of the real anthroposol sample, determined by X-ray Powder Diffraction (XRD), total organic carbon (TOC) measurement and extraction methods. The effect of different initial Cr(VI) concentrations (2×10^{-2}, 5×10^{-4}, 10^{-4}, 10^{-5}, and 10^{-6} M), background electrolyte (10^{-3}, 10^{-2}, and 10^{-1} M KNO_3), pH values (3–9), and sorbate/sorbent ratios (2 g/L - 20 g/L) were investigated. Maghemite and ferrihydrite were confirmed to be the main phases controlling Cr(VI) adsorption with increasing Cr(VI) concentration. Humic acids were primarily responsible for Cr(VI) reduction, especially at low pH values. The reduction of Cr(VI) was also proved in case of illite and kaolinite by XAS and isotopic analyses. Illite revealed higher reduction capacity in comparison with kaolinite based on XAS measurements. Chromium isotopic fractionation, resulting from Cr(VI) reduction, was the highest in the case of humic acids, followed by kaolinite and illite. However, a dissolution of intrinsic Cr originally present within kaolinite and illite might affect the final Cr isotopic composition of the supernatants due to its different Cr isotopic signature. In general, the combination of three different approaches was confirmed to offer more comprehensive information about Cr(VI) adsorption and/or reduction in soils. Detailed studies using soil mixtures can help to predict how the soil components affect Cr(VI) behavior in natural soils and possibly could improve the environmental remediation processes.

1. Introduction

Toxic properties of mobile and soluble Cr(VI) and its environmental impact are already well-known and widely published (Gunkel-Grillon et al., 2014; McDermott et al., 2015; Mishra and Bharagava, 2016; Mollon et al., 2016; Shadid et al., 2017). Currently, attention is turned more to the development of promising techniques capable of removing Cr(VI) from contaminated soils and waters with remediation measures (Dinker and Kulkarni, 2015; Jamieson-Hanes et al., 2015; Jin et al., 2016; Li et al., 2018; Pradhan et al., 2017; Wu et al., 2016).

The binding mechanisms of Cr(VI) in soils are of considerable interest prior to any remediation process. The distribution of Cr(VI) and the rate of its transport in soils are determined to a large extent by the adsorption to soil components (Gustafsson, 2009). Thermodynamically based surface complexation models (SCMs) appeared to be a great predictive research tool for describing metal behavior in natural systems (Koretsky, 2000; Reich and Koretsky, 2011). Since the SCMs have been used to describe Cr(VI) adsorption onto individual soil

* Corresponding author.
E-mail address: veselskav@fzp.czu.cz (V. Veselská).
[1] Present address: Department of Chemistry, Faculty of Basic Sciences and Humanity, Lingaya's University, Faridabad, Haryana, INDIA-121002.
[2] Present address: Department of Environmental Engineering, Institute of Chemical Process Fundamentals of the CAS, v. v. i., Rozvojová 135/1, CZ-16502, Prague, Czech Republic.

https://doi.org/10.1016/j.envint.2019.03.066
Received 30 November 2018; Received in revised form 26 February 2019; Accepted 27 March 2019
Available online 07 May 2019

components (Komárek et al., 2015; Koretsky, 2013; Reich and Koretsky, 2011; Xie et al., 2015), their development and application in soils is still challenging due to the heterogeneity and complexity of soil systems. To date, only a limited number of studies have been carried out on natural soils to predict Cr(VI) retention and partitioning using mainly the CD-MUSIC model (Gu et al., 2017; Pérez et al., 2014). Pérez et al. (2014) described Cr(VI) adsorption on ferralic soil, highlighting the role of natural iron oxides present and the similarity of the adsorption behavior of Cr(VI) to the behavior exhibited by synthetic iron oxides. Likewise, Gu et al. (2017) confirmed crystalline and amorphous iron oxides and hydroxides to be the soil components with the most important reactive surfaces for Cr(VI) retention in soils. To simplify the modeling calculations, the contributions of silicates or organic matter were neglected in the prior modeling attempts in soils. Additionally, the 2-pK models such as the constant capacitance model (CCM), the diffuse double layer model (DLM) or the triple layer model (TLM) for soils or even for soil component mixtures are lacking.

Whereas adsorption represents one of the processes of natural attenuation of Cr(VI) in the subsurface environment including soils, the rapid reduction of Cr(VI) to Cr(III), in particular by organic matter commonly found in soils, occurs immediately after Cr(VI) release into the soil (Kožuh et al., 2000). At present, the redox transformations of Cr (VI) *in situ* are studied particularly by a wide variety of synchrotron X-ray techniques, which are able to provide information about speciation and short-range structure of Cr in soils (Ginder-Vogel and Sparks, 2010; Hausladen and Fendorf, 2017; Hopp et al., 2008; Hori et al., 2015; Hsu et al., 2015; Jardine et al., 2013; Rinehart et al., 1997). Since reduction of Cr(VI) to Cr(III) is known to be accompanied by Cr isotopic fractionation (Ellis et al., 2002; Izbicki et al., 2008; Zink et al., 2010), Cr isotopic composition in sediments and soils can provide a useable tool for monitoring and quantifying the extent of reduction (Bauer et al., 2018). However, most of the prior studies using stable Cr isotopes for tracking redox processes in subsurface and surface environments were focused mainly on the treatment of groundwaters, rivers, seawaters and run-offs (Blowes, 2002; Bullen, 2007; Economou-Eliopoulos et al., 2014; Ellis et al., 2002; Farkaš et al., 2013; Novak et al., 2014, 2017, 2018; Zink et al., 2010), mostly using electron donors such as organic molecules and aqueous Fe(II) (Kitchen et al., 2012), bacterial species (Basu et al., 2014; Xu et al., 2015) or Fe-based permeable reactive barrier materials (Basu and Johnson, 2012; Wanner et al., 2012). There is a lack of studies using the Cr isotopic system for monitoring the accompanying redox processes during Cr(VI) adsorption onto the surfaces of clay minerals or organic substances in soils. Although nonredox reactions including adsorption tend to have negligible isotopic effect (Ellis et al., 2004), redox reactions cause changes in the local bonding environment of Cr(VI) (Quin and Wang, 2017). Thus, Cr isotopic fractionation during adsorption of Cr(VI) onto different soil components points to the aligned redox processes and consequently provides a suitable tool for the distinction between adsorption and reduction.

The main aim of this study is to investigate redox transitions associated with the adsorption of Cr(VI) on commonly occurring soil components and their synthetic mixtures with a composition reflecting the real anthroposol sample. This study emphasizes a multidisciplinary approach by coupling the mechanistic surface complexation modeling with spectroscopic and isotopic analyses. Combination of these three approaches can provide more comprehensive information about the real processes of Cr(VI) adsorption and/or reduction in soils. To assess the dominant soil component responsible for Cr(VI) retention in mixtures, a component additivity approach has been tested by applying 2-pK DLM parameters, derived for single components including oxides, silicates and humic acids, to multicomponent mixtures. To obtain a more detailed insight into accompanying redox processes, focusing mainly on the role of humic acids and clay minerals, X-ray absorption spectroscopy and isotopic analyses have been performed.

Table 1
Composition of soil component mixtures M1-M4 (presented in wt%).

	Quartz	Albite	Illite	Kaolinite	Maghemite	Ferrihydrite	Humic acids
M1	88.6	5.4	3.0	1.4	1.6	–	–
M2	86.4	5.3	2.9	1.4	1.6	2.4	–
M3	76.6	4.7	2.6	1.2	1.4	2.4	11.1
M4	78.8	4.8	2.7	1.2	1.4	–	11.1

2. Materials and methods

2.1. Synthetic soil component mixtures

The natural clay and feldspar minerals, namely, kaolinite (KGa-2), illite (IMt-2) and albite, were purchased from the Clay Minerals Repository (Clay Minerals Society, Warren County, Georgia, USA and Silver Hill, Jefferson Canyon, Montana, respectively) and LB Minerals, s.r.o. (Slovakia), respectively. The micromilled silica sand (middle grain size from 6 to 9 μm) with SiO_2 content above 99% was purchased from Sklopísek Střeleč Company. Humic acids (technical grade) and maghemite (nano powder, < 50 nm fraction) were obtained from Sigma Aldrich. 2-Line ferrihydrite was synthesized by rapid hydrolysis of 0.2 M $Fe(NO_3)_3 \cdot 9\ H_2O$ solution at 25 °C by titrating the solution with 1 M KOH to pH = 7.18 under vigorous stirring (Schwertmann and Cornell, 2000). The original solid phase was filtered, washed with 300 mL of distilled water 4–5 times, air-dried, and then grounded and stored for further use.

The mixtures of soil components were prepared to reflect the composition of real anthroposol samples (Table 1). For this reason, the basic mixture of soil components (M1) was created on the basis of the percentage of crystalline phases of a natural soil that were quantified by X-ray Powder Diffraction (XRD) with Rietveld analysis (see Supporting information, Table S1). In addition, mixtures containing humic acids and ferrihydrite were prepared based on total organic carbon content and amorphous inorganic Fe content in natural soil, respectively (Table S2). Complete soil characteristics and composition are described in detail in SI (Tables S1, S2).

2.2. Adsorption experiments

2.2.1. Adsorption batch experiments prior to adsorption modeling

Series of adsorption edge experiments have been performed under atmospheric conditions on soil component mixtures as well as on single soil components. A set of batches with either 250 or 500 mL solution of Cr(VI) at initial concentrations of 10^{-4}, 10^{-5}, and 10^{-6} M and background electrolyte (10^{-3}, 10^{-2}, and 10^{-1} M KNO_3) was prepared in polycarbonate centrifuge bottles (Thermo Fisher Scientific). Either mixtures of selected soil components described in Table 1 (20 g/L) or single components including kaolinite, illite, albite (20 g/L) and quartz, ferrihydrite, maghemite, humic acids (2 g/L) were then added and kept in suspension by shaking for 24 h on orbital shaker (GFL 3005) at 200 rpm at 25 °C. After equilibration, the adsorption of Cr(VI) was measured as a function of pH (3–9), while the pH range for modeling purposes was chosen to capture the variable pH conditions. The pH value was gradually adjusted by adding either NaOH or HNO_3 (10^{-3}, 10^{-2}, and 10^{-1} M) starting at pH value 3 in steps of ~0.5 pH until pH 9 was reached. A 10-mL aliquot of the slurry was removed after each step and was subjected to constant agitation at 200 rpm on a programmable rotator (Multi RS-60) for a further 24 h. Subsequently, pH was measured, and all the samples were centrifuged (UNIVERSAL 320 centrifuge, 10 min, 3000 rpm), filtered (0.2 μm, regenerated cellulose) and the supernatants were analyzed using inductively coupled plasma optical emission spectrometry (ICP-OES, Agilent Technologies 730 Series, USA). The adsorbed Cr(VI) was calculated by subtracting the amount of Cr(VI) in the supernatant from the total added Cr(VI).

Table 2
Surface properties, 2-pK DLM parameters and inner-sphere complexation reactions of Cr(VI) on the pure soil component-solution interface (median values of constants optimized in FITEQL 4.0). Protonation and deprotonation constants were optimized in ProtoFit 2.1.

	Quartz	Albite	Humic acids	Maghemite	Kaolinite[b]	Illite[b]	Ferrihydrite[b]
Protonation and deprotonation	Log K						
$>XOH + H^+ \rightleftharpoons >XOH_2^+$	−3.92	−4.67	5.48	5.71[a]	−1.93	−4.29	7.01
$>XOH \rightleftharpoons >XO^- + H^+$	−7.07	−1.08	8.09	−7.74[a]	−6.59	−8.99	−7.86
Monodentate inner-sphere complexes	Log K						
$>XOH + CrO_4^{2-} + H^+ \rightleftharpoons >XCrO_4^- + H_2O$	8.41	11.9	22.8	11.2	9.50	7.47	12.3
Site density (sites/nm^2)	476	34.8	167	2.28[a]	3.89	216	0.73
Specific surface area (m^2/g)	1.60	1.10	0.98	37.0	15.8	16.5	323

[a] Komárek et al. (2015).
[b] Veselská et al. (2016).

2.2.2. Adsorption batch experiments prior to spectroscopic investigations and isotopic measurements

The adsorption experiments prior to X-ray absorption spectroscopy (XAS) were performed during 24 h on mixture M1 (silicates with maghemite), M3 (silicates, maghemite, ferrihydrite and humic acids) and M4 (silicates with maghemite and humic acids) as well as on single phases of illite, kaolinite and humic acids (20 g/L) in 500 mL of electrolyte at the concentration of 10^{-2} M KNO_3, initial Cr(VI) concentration of 5×10^{-4} M and pH of 4 and 6.5. The higher Cr initial concentration in comparison with concentration prior to adsorption modeling was calculated according to the adsorption capacities of the adsorbents, to achieve a sufficient Cr concentration for spectroscopic analyses (data not shown). Additionally, adsorption experiments on clay minerals were performed at even higher initial Cr(VI) concentration (2×10^{-2} M). The pH value of this experiment was determined by the highest adsorption efficiency of clay minerals and was adjusted to 6 and 4.5 for kaolinite and illite, respectively. For isotopic measurement purposes, aimed at assessing the main Cr(VI) reductants, adsorption batch experiments were performed in duplicate over 24 h on illite, kaolinite and humic acids (20 g/L) in 250 mL of electrolyte at the concentration of 10^{-2} M KNO_3, initial Cr(VI) concentration of 10^{-4} M and pH of 4, 6.5 and 9. As pH is a dominant factor affecting the solubility and mobility of Cr(VI) in soils, pH values were selected as representatives of slightly acidic, neutral and highly alkaline conditions.

Consequently, a 2×10 mL aliquot of the solution was removed from each batch before adding a solid phase to measure an initial Cr concentration. A 2×10 mL aliquot of the slurry was removed after adsorption, centrifuged and filtered to analyze supernatants using ICP-OES. The rest of the slurry was subsequently filtered using a vacuum pump (filter DIA 90 mm; 84 g/m^2) and the solid phase was frozen prior to further freeze-drying (24 h). Freeze-dried samples were either stored for further spectroscopic analysis or dissolved for isotopic measurements (see SI).

2.3. Modeling approach

2.3.1. Surface protonation modeling

To optimize the values of surface protonation constants and the total number of surface sites for quartz, albite and humic acids, the titrations of the single soil component-H^+ systems were carried out. Acid-base potentiometric titrations were performed on the soil component suspensions (12.5 g/L, Jolsterå et al., 2010) at ionic strength values of 10^{-3}, 10^{-2}, and 10^{-1} M using $NaNO_3$ as a background electrolyte. For quartz, the optimization of surface protonation constants was performed at 10^{-1} M ionic strength only. Subsequently, values were compared with previously published parameters for quartz (Komárek et al., 2015). Suspensions were titrated by 10^{-2} M HNO_3/NaOH (albite and quartz) or 10^{-1} M HNO_3/NaOH (humic acids) under constant stirring and N_2 atmosphere (Jolstera et al. 2010) using the automatic TitroLine® alpha plus Titration Unit (Schott, Germany). Forward and back titration datasets within each ionic strength were used either individually or simultaneously to optimize the 2-pK DLM parameters using the program ProtoFit (Turner and Fein, 2006) and assuming surface reactions (Eqs. (1), (2)):

$$>XOH + H^+ \rightleftharpoons >XOH_2^+ \ \log K_1 \quad (1)$$

$$>XOH \rightleftharpoons >XO^- + H^+ \ \log K_2 \quad (2)$$

The average of the best fits for each ionic strength 2-pK DLM parameters was used for further modeling. Titration data and corresponding models for quartz, albite and humic acids are presented in Fig. S1.

Model parameters for maghemite and ferrihydrite, kaolinite and illite were taken from Komárek et al. (2015) and Veselská et al. (2016), respectively.

2.3.2. Surface complexation modeling

Adsorption edge data as well as 2-pK DLM parameters derived from Protofit were used to obtain Cr(VI) surface complexation constants and calibrate the model. The reactive surface areas (SA) of soil components and their mixtures were determined by the layered adsorption BET isotherm obtained from measurements of N_2 adsorption isotherms using ASAP 2020 and ASAP 2050 surface area analyzers (Micromeritics, USA). Surface complexation constants of Cr(VI) for quartz, albite, humic acids and maghemite were optimized in FITEQL 4.0 (Herbelin and Westall, 1999) with the default thermodynamic data for aqueous species from the database of Visual MINTEQ 3.0 (Gustafsson, 2013). The single monodentate inner-sphere surface site complexes have been considered for each of those phases. The average surface protonation constants estimated from titration data were used. The final 2-pK DLM prediction was calculated by thermodynamic database program Visual MINTEQ 3.0 using median stability constants of surface complexes (Table 2). The goodness of fit of each calculated model prediction to the experimental data was assessed using the WSOS/DF ratio produced by the software. Individual stability constants and the errors for the 2-pK DLM best fits are summarized in Table S3. The intrinsic binding constants of Cr(VI) onto ferrihydrite, kaolinite and illite were taken from our previous work (Veselská et al., 2016).

For soil component mixtures M1-M4, a component additivity 2-pK DLM, using acidity constants and equilibrium constants determined for each pure phase, was used for prediction of Cr(VI) adsorption using a multisurface complexation model. Total Cr(VI) adsorbed in the mixtures was described either by stability constants of the dominant soil component or the combination of stability constants of phases, which was attributed to the best fit of the model for the Cr(VI) adsorption data.

2.4. Spectroscopic analyses

2.4.1. X-ray absorption spectroscopy (XAS)

Cr *K*-edge X-ray absorption spectra were collected at the SUL-X (untreated clay minerals, reference materials) and XAS beamlines (Cr-loaded humic acids, clay minerals, synthetic mixtures of soil minerals)

of the synchrotron light source of the Karlsruhe Institute of Technology, Germany, using a silicon (111) double crystal monochromator with fixed beam exit. Because SUL-X is a beamline with a wiggler as the radiation source, the samples sensitive to beam-induced changes, namely, the ones from the adsorption experiments with humic acid and clay minerals, have been measured at the XAS beamline as described in the SI. Cr *K*-edge spectra were collected at the SUL-X beamline with a step width of 5 eV from −150 to −50 eV, 2 eV from −50 to −20 eV below the edge, 0.3 eV between ± 20 eV relative to the edge, and with k steps 0.05 $Å^{-1}$ to k 12 $Å^{-1}$ above the absorption edge with measurement times multiplied by $k^{0.5}$. Increasing the detector integration times with $k^{0.5}$ has been chosen as a compromise between acceptable overall measurement times and statistics in the EXAFS regime. At the XAS beamline, step size between ± 20 eV relative to the edge was 0.5 eV, maximum k was 16 $Å^{-1}$, but data were not usable beyond k 12 $Å^{-1}$ due to numerous severe X-ray diffraction effects that could not be suppressed. Several spectra have been measured for each sample and reference substances to check for beam-induced changes, and only the unaffected scans have been used and were averaged. All XAS spectra have been pre- and post- edge corrected, normalized to an edge jump of one, and energy calibrated by the Athena software (Ravel and Newville, 2005). If no beam-induced changes have been observed on the spectra at the same sample measuring position, all scans have been merged prior to linear combination fitting (LCF) with references. In the case of recognizable beam-induced Cr(VI) reduction, only the first scan of each scan series was used for merging (in case of kaolinite and M1) (Figs. S2, S3).

LC-Fits of Cr *K*-XANES reference spectra have been applied to quantitatively determine the Cr(VI)/Cr(III) ratios in samples using the Athena software. As references for Cr(VI), $K_2Cr_2O_7$, $PbCrO_4$ and Cr(VI)-loaded ferrihydrite were available. For Cr(III), $Cr(NO_3)_3 \times 9H_2O$ as well as Cr(VI)-treated illite at pH 6.5 with all Cr present as Cr(III) and illite where the Cr(VI) has been reduced to Cr(III) with the synchrotron beam of high photon density at the SUL-X beamline were used. Additionally, the Cr(VI)-treated humic acids where all Cr(VI) was reduced to Cr(III) have been used as a Cr(III) reference for the mixtures containing humic acids. Cr *K*-XANES spectra of illite, kaolinite and humic acids before adsorption experiments have also been included in LC-Fits if they revealed only Cr(III).

Due to lack of pure Cr(VI) references based on illite and kaolinite and partly also Cr(III) references, the intrinsic Cr(III) has not been reproduced well from the LC-Fits of clay minerals and humic acids. Therefore, LC-Fits of spectra of these samples containing both initial and adsorbed Cr fractions were used for subtraction of the intrinsic Cr according to the Cr concentration (ppm) before and after adsorption (Table S4). Prior subtraction of the intrinsic Cr-weighted spectral fraction was not used due to spectral artifacts.

2.4.2. Fourier transform infrared spectroscopy (FTIR)

FTIR spectra of the humic acids in KBr pellets were measured with a Nicolet Avatar 360 spectrometer with a room temperature DTGS detector. The resolution was set at 1.93 cm^{-1} in the spectral region 400–4000 cm^{-1}, and 200 scans were collected using the software OMNIC 4.1.

2.5. Cr isotopic analysis

Supernatants and dissolved solid samples after adsorption of Cr(VI) (see Section 2.2.2) were subjected to Cr(VI) separation from the matrix using a modified anion exchange chromatography method prior to Cr isotopic analysis (Bullen, 2007; Šillerová et al., 2014), as detailed in the SI. All Cr isotopic measurements were performed on a multicollector inductively coupled plasma mass spectrometer (MC ICP-MS, Neptune, Thermo, Germany) equipped with nine Faraday cups (see SI). Corrections for mass bias were performed using a double-spike method involving spiking of sample with solution enriched in two isotopes (^{50}Cr and ^{54}Cr). The results were related to the Cr standard NIST SRM 979 and reported as relative deviations in parts per mil (‰) (Eq. (3)). The $\delta^{53}Cr$ value of NIST 979 doped with a double spike was monitored over the course of our study and the average value was −0.001 ± 0.054(2SD) (n = 12). The isotopic composition of all samples was corrected to this value.

$$\delta^{53}Cr = \frac{^{53}Cr/^{52}Cr(sample)}{^{53}Cr/^{52}Cr(SRM979)} - 1\ (‰) \tag{3}$$

The relative isotopic difference Δ between reactant, initial $K_2Cr_2O_7$ solution (lq1), and product, supernatant after adsorption (lq2) was calculated according to Eq. (4):

$$\Delta^{53/52}Cr(lq1 - lq2) = \delta^{53}Cr(lq1) - \delta^{53}Cr(lq2) \tag{4}$$

2.5.1. Mass balance

To verify and evaluate the isotopic and concentration data, the Cr concentrations and δ^{53} Cr values were determined in all "inputs" and "outputs" of the experiment. According to the mass conservation law, the inputs must equal the outputs. The inputs include Cr in the initial $K_2Cr_2O_7$ solution (in Eq. (5) numbered as 1) and the intrinsic Cr in the solid phases (2). The outputs include Cr in the supernatant (3) and Cr in the solid phases (4) after adsorption. Consequently, the mass balance equation was applied:

$$m_1\delta_1^{53}Cr + m_2\delta_2^{53}Cr = m_3\delta_3^{53}Cr + m_4\delta_4^{53}Cr \tag{5}$$

where m_1 is the mass (mg) of total Cr in the initial solution, m_2 is the mass (mg) of total intrinsic Cr in the solid sample, m_3 is the mass of total Cr (mg) in the supernatants after adsorption and m_4 is the mass of total Cr (mg) adsorbed on the solid sample. The $\delta_1{}^{53}Cr$, $\delta_2{}^{53}Cr$, $\delta_3{}^{53}Cr$, $\delta_4{}^{53}Cr$ are the Cr isotopic fractionation ratio (‰) of the initial solution, intrinsic Cr, supernatant and solid phase after adsorption, respectively.

3. Results and discussion

3.1. Role of maghemite and ferrihydrite in Cr(VI) adsorption

Developing robust SCMs for Cr(VI) in mixtures of soil components was carried out to determine the leading soil component responsible for Cr(VI) retention in the mixtures. A dominant role of common ferric oxides and (oxy)hydroxides during Cr(VI) adsorption was anticipated. For the purpose of this study, 2-pK DLM was chosen as an intermediate approach, with relatively few fit parameters, while trying to obtain internally-consistent data parameterized by using the same simplified modeling framework for all soil constituents.

3.1.1. Mixture M1: effect of maghemite

In general, a component additivity approach was used for the mixture consisting of quartz, albite, illite, kaolinite and maghemite using the 2-pK DLM and excluding the contribution of surfaces of quartz, albite, kaolinite or illite to adsorption of Cr(VI) *via* inner-sphere complexes. When replacing a small percentage of maghemite (1.6 wt%, Table 1) by quartz, no performance of the model and a strong dependence of Cr(VI) adsorption on the ionic strength within a mixture of silicates was confirmed (Fig. S4a). Adsorption of Cr(VI) at lower Cr loadings is ionic strength-dependent, which indicates impact of (phylo) silicates through the formation of outer-sphere complexes that could not be described by the simple 2-pK DLM (Ajouyed et al., 2011; Koretsky, 2013; Veselská et al., 2016). The role of maghemite as a main mineral phase controlling Cr(VI) adsorption was highlighted at initial total Cr(VI) concentration of 10^{-4} M, while the 2-pK DLM was found to fit the adsorption edge data quite well just taking into account inner-sphere monodentate complexes for maghemite (Fig. 1a). Model simulations slightly overestimated Cr(VI) adsorption up to pH 7, even when considering the same ratio of the soil components in M1 (20 wt% of each) (Fig. S4b). This refers to the limited model ability to capture

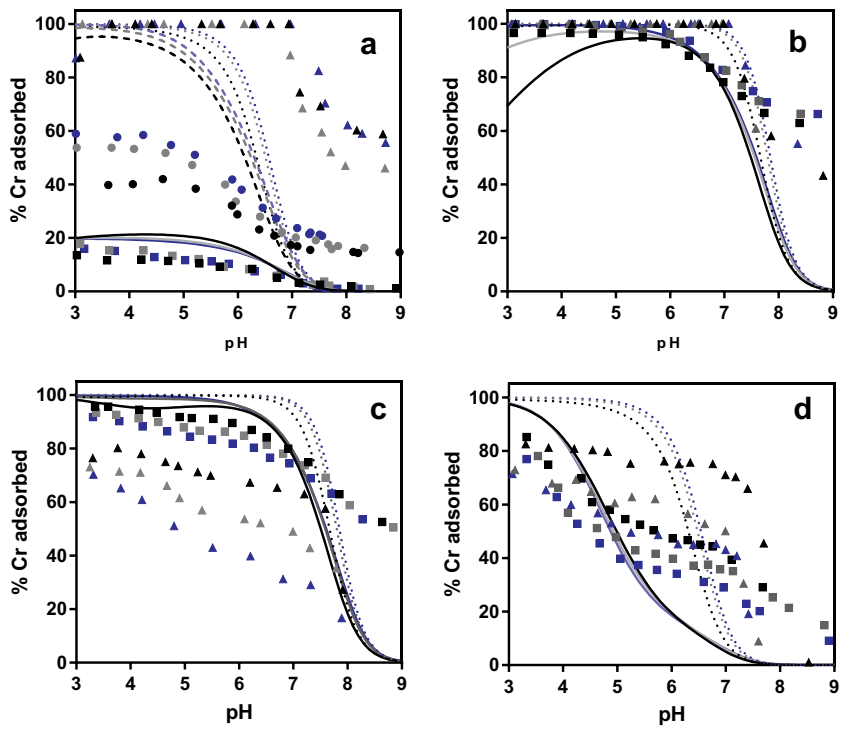

Fig. 1. Adsorption of Cr(VI) onto 20 g/ L M1 (a), M2 (b), M3 (c) and M4 (d) at 10^{-4} M (square) 10^{-5} (circle) and 10^{-6} M (triangle) Cr(VI) and with 10^{-1} M (black), 10^{-2} M (grey) and 10^{-3} M (blue) KNO_3 modeled using the 2-pK DLM (solid, dashed and dotted lines at 10^{-4} M, 10^{-5} M and 10^{-6} M Cr (VI), respectively). (For interpretation of the references to colour in this figure legend, the reader is referred to the web version of this article.)

simultaneously processes, such as formation of coatings on the surfaces of individual phases, site-blocking and dissolution of silicates. Silicates releasing from Si–bearing minerals and adsorbing on surfaces of iron oxides could compete with the Cr(VI) as already observed by Jolsterå et al. (2010) or Kamagaté et al. (2016). This effect was not considered in the present model. Likewise, cations incorporated as impurities in the structure of Fe oxides or oxyhydroxides could suppress the availability of inner-sphere binding sites for Cr(VI) oxyanions (Johnston and Chrysochoou, 2016).

3.1.2. Mixture M2: effect of ferrihydrite

The adsorption data for Cr(VI) in M2 (silicates, maghemite, ferrihydrite) have been sufficiently described by monodentate complexes on the surfaces of maghemite and ferrihydrite and adding ferrihydrite improved the model fit in M2 at 10^{-6} M Cr(VI) in comparison with M1 (without ferrihydrite) (Fig. 1b, Table 1). Likewise, at 10^{-4} M Cr(VI), total amount of Cr(VI) adsorbed increased significantly due to sorption onto both maghemite and ferrihydrite surfaces and 2-pK DLM fits the data in a range of pH typical for natural soils, from 5 to 7. Under acidic conditions, predominant contribution of bidentate complexes also needs to be taken into account considering surfaces of Fe oxyhydroxides (Xie et al., 2015; Veselská et al., 2016).

3.1.3. Mixtures M3 and M4: effect of maghemite and ferrihydrite in the presence of humic acids

Adsorption of Cr(VI) in M3 was attributed to reactive surfaces of humic acids, ferrihydrite and maghemite (Fig. 1c). Total Cr(VI) adsorbed could be attributed to the surface of maghemite and humic acids in the case of M4 (Fig. 1d). The prevalent role of humic acids is highlighted at low initial Cr(VI) concentration, where their presence both limits adsorption capacity of other soil components due to formation of coatings on their surfaces (Al-Essa and Khalili, 2018; Chen et al., 2017; Jiang et al., 2014) and limits the 2-pK DLM capability to describe Cr(VI) adsorption due to its restraint to capture the reduction of Cr(VI) by humic acids. On the other hand, increasing the initial Cr concentration in the solution increases the adsorbed Cr(VI) amount in M3 with ferrihydrite. Adsorption data are fitted by the 2-pK DLM with slight overestimation up to pH 7, emphasizing a significant contribution of ferrihydrite to Cr(VI) adsorption. In summary, the role of Fe oxides and (oxy)hydroxides in Cr(VI) adsorption is crucial, and they represent phases controlling Cr(VI) behavior in soils, especially those with low organic matter content.

3.2. Role of clay minerals and humic acids in Cr(VI) reduction

Among available Cr(VI) reductants, clay minerals as well as humic acids were considered to be involved in redox processes, which accompanied Cr(VI) adsorption onto soil component mixtures. Therefore, they were further investigated by XAS, FTIR and isotopic analyses in order to evaluate the extent of Cr(VI) reduction.

3.2.1. Effect of intrinsic Cr

In general, Cr(VI) fractions adsorbed onto illite, kaolinite and humic acids were calculated from linear combination fits (LCFs) of Cr *K*-XANES spectra containing both intrinsic Cr(VI)/Cr(III) and adsorbed Cr (VI)/Cr(III) fractions (Table 3). The results of LCF underline the important impact of the intrinsic Cr fraction on total Cr(VI) adsorbed on clay minerals at low initial Cr(VI) concentration. In case of illite, the small amount of adsorbed Cr(VI), comparable to amounts of intrinsic Cr, prevents estimation of a Cr(VI) reduction extent. Effect of intrinsic Cr can be clearly seen also in the case of kaolinite, where concerning lower Cr(VI) concentration, approximately 31% and 27% of the total Cr after adsorption, represent initial Cr fractions at pH 4 and 6.5, respectively (Table 3, II). Evaluation of isotopic data is aggravated also by the presence of intrinsic Cr within kaolinite and illite (Table S4). Nevertheless, the presence of intrinsic Cr within individual soil components simulates better the real conditions in soils. The isotopic signature of the intrinsic Cr in kaolinite and illite is different (δ^{53}Cr = 0.193 ± 0.04‰ and δ^{53}Cr = −0.317 ± 0.02‰, respectively) in comparison with the initial Cr solution (δ^{53}Cr = −0.475 ± 0.02‰; Table 4). Therefore, two isotopically different sources of Cr are mixed during Cr(VI) adsorption.

No intrinsic Cr(III), as confirmed by XAS, was desorbed from clay minerals in the blank experiment. However, a partial dissolution of the intrinsic Cr(III) during Cr(VI) adsorption experiments cannot be excluded and the final Cr isotopic composition in the supernatants can be

Table 3
(I.) LC-Fit of Cr *K*-XANES spectra containing both, intrinsic and adsorbed spectral fractions; (II.) adsorbed Cr(VI)/Cr(III) fractions calculated after subtraction of intrinsic Cr; (III.) re-normalized Cr(VI)/Cr(III) ratios of adsorbed Cr (Cr(VI)ads + Cr(III)ads = 100%). Considering clay minerals at the higher Cr initial concentration, the pH of the adsorption experiment was chosen taking into account the highest adsorption capacity of the adsorbents.

Adsorption experiment	pH	Analytical treatment	Cr(VI) %		Cr(III) %	
			Ads.	Intr.	Ads.	Intr.
Kaolinite initial				7.90		92.1
Kaolinite after adsorption	4	I.	37.7		62.3	
(5×10^{-4} M Cr(VI))		II.	35.2	2.50	33.4	28.9
		III.	51.3		48.7	
	6.5	I.	55.1		44.9	
		II.	53.0	2.10	20.0	24.9
		III.	72.6		27.4	
Kaolinite after adsorption	6.5	I.	82.1		17.9	
(2×10^{-2} M Cr(VI))		II.	81.9	0.20	15.3	2.60
		III.	84.3		15.7	
Illite initial				0.00		100
Illite after adsorption	4	I.	4.70		95.3	
(5×10^{-4} M Cr(VI))		II.	4.70	0.00	10.4	84.9
		III.	31.1		68.9	
	[a]6.5	I.				100
Illite after adsorption	4	I.	37.5		62.5	
(2×10^{-2} M Cr(VI))		II.	37.5	0.00	37.3	25.2
		III.	50.1		49.9	
Humic acids initial				0.00		100
Humic acids after	4	I.	0.00		100	
adsorption		II.	0.00	0.00	96.9	3.06
(5×10^{-4} M Cr(VI))		III.	0.00		100	
	6.5	I.	0.00		100	
		II.	0.00	0.00	95.5	4.53
		III.	0.00		100	
Mixtures of soil components						
M1	4	I.	57.0		43.0	
(5×10^{-4} M Cr(VI))	6.5	I.	35.0		65.0	
M3	4	I.	50.0		50.0	
(5×10^{-4} M Cr(VI))	6.5	I.	64.0		37.0	
M4	4	I.	1.50		98.5	
(5×10^{-4} M Cr(VI))	6.5	I.	1.20		98.8	

[a] No LCF, no Cr(VI) adsorption, 100% Cr(III) = intrinsic Cr.

affected by isotopic signature of this intrinsic Cr. Hence, combination of XAS and isotopic analyses constitutes a very powerful tool for understanding the mechanism of Cr(VI) reduction during adsorption onto soil minerals.

Unlike clay minerals, the intrinsic Cr(III), originally present in humic acids represents a small percentage of the total Cr(III) (Table 3) and modifies the XANES spectrum of Cr-loaded samples insignificantly. XANES analysis of raw humic acids confirms the absence of a pre-edge peak in the spectrum of intrinsic Cr, thus indicating the presence of octahedrally coordinated Cr(III) in the first shell (Jiang et al., 2014; Peterson et al., 1996). However, the features in Cr *K*-edge XANES spectra of intrinsic Cr and Cr adsorbed to humic acids differ, which suggests a different arrangement of octahedral Cr(III) in functional groups of humic acids due to the reduction of Cr(VI) by the humic acids.

3.2.2. The ability of clay minerals to reduce Cr(VI)

The adsorbed Cr species, calculated by subtraction of intrinsic Cr fractions from total Cr, were renormalized and resulted in approximately 51% of adsorbed Cr(VI) and 49% of adsorbed Cr(III) in the case of Cr-loaded kaolinite at initial Cr(VI) concentration of 5×10^{-4} M and pH 4 (Table 3, III). The extent of Cr(VI) reduction decreased with increasing pH, reaching approximately 73% of adsorbed Cr(VI) and 27% of adsorbed Cr(III) at pH 6.5. Considering the highest adsorption efficiency of the kaolinite at pH 6.5, up to 84% of the adsorbed Cr remains as Cr(VI) at higher initial Cr(VI) concentration (2×10^{-2} M).

In case of illite, the adsorbed Cr(VI) fraction was very low at pH 4 representing up to 15% of the total Cr after adsorption and zero at pH 6.5. After renormalization, the adsorbed Cr(VI) represents only 31% at pH 4. The extent of reduction can be evaluated better at higher Cr (VI) loading (2×10^{-2} M), where 75% of total Cr is adsorbed at pH 4, but about approximately half of this is reduced to Cr(III). Illite used in this study contains mixed Fe(II, III) (Fig. S5), allowing structural Fe(II) to be involved in Cr(VI) reduction (Borisover and Davis, 2015; Joe-Wong et al., 2017; Taylor et al., 2000). Assuming that the 50% of Cr(III) (78 ppm) is completely reduced by the structural Fe(II), a shift in the Fe *K*-edge position in XANES spectra would not be recognizable because the required oxidation of about 233 ppm Fe is smaller than 1.5% of the total Fe. Therefore, in the case of illite, Cr(VI) reduction can take place by oxidation of Fe(II) to Fe(III) (Stucki, 2013; Vinuth et al., 2015), although this effect is too small to be observed as an Fe *K*-edge shift. Excluding the effect of structural Fe(II), some potential for Cr(VI) reduction may be attributed to little adsorbed Fe(II) or organic matter on the surfaces of clay minerals (Kwak et al., 2018). Both, kaolinite and illite were used as received without any additional purification prior to adsorption experiments in order to simulate better the natural conditions in soils. Therefore, traces of impurities can also play a role in reducing processes on clay minerals. Based on XRD results of kaolinite used in this study (Veselská et al., 2016), traces of TiO_2 were confirmed. These might cause photocatalytic reduction of Cr(VI) in aqueous environments, as has been widely discussed in previous studies (Ahmed et al., 2018; He et al., 2013), working under similar experimental conditions (pH, Cr(VI) concentration, TiO_2 concentration) as in our case.

Isotopic analysis proved Cr isotopic fractionation caused by reduction of Cr(VI) to Cr(III) for both clay minerals although the changes in δ^{53}Cr were relatively low (kaolinite) or even negligible (illite). Isotopically heavier Cr(VI) fraction remaining in the supernatants after adsorption relative to the initial Cr(VI) fraction in the $K_2Cr_2O_7$ solution was confirmed due to Cr(VI) reduction. More significant changes were observed in the presence of kaolinite, especially for the initial pH 4 and

Table 4
Cr isotopic data for the kaolinite, illite and humic acid. $\delta^{53}Cr_{init}$ = initial $K_2Cr_2O_7$ solution, $\delta^{53}Cr_{intr}$ = intrinsic Cr in the samples, $\delta^{53}Cr_{eq}$ = supernatants after adsorption, $\Delta^{53/52}Cr_{(lq1\text{-}lq2)}$ = relative isotopic difference (‰).

	Initial pH	$\delta^{53}Cr_{init}$ ± 2SD	$\delta^{53}Cr_{intr}$ ± 2SD	$\delta^{53}Cr_{eq}$ ± 2SD	$\Delta^{53/52}Cr_{(lq1\text{-}lq2)}$
Kaolinite	4	−0.475 ± 0.020	0.193 ± 0.040	−0.217 ± 0.081	−0.258
	6.5	−0.475 ± 0.020	0.193 ± 0.040	−0.209 ± 0.056	−0.266
	9	−0.475 ± 0.020	0.193 ± 0.040	−0.346 ± 0.044	−0.129
Illite	4	−0.475 ± 0.020	−0.317 ± 0.016	−0.398 ± 0.004	−0.077
	6.5	−0.475 ± 0.020	−0.317 ± 0.016	−0.431 ± 0.027	−0.044
	9	−0.475 ± 0.020	−0.317 ± 0.016	−0.632 ± 0.075	0.157
Humic acid	4	−0.475 ± 0.020	−0.524 ± 0.059	0.039 ± 0.066	−0.514
	6.5	−0.475 ± 0.020	−0.524 ± 0.059	−0.185 ± 0.007	−0.29
	9	−0.475 ± 0.020	−0.524 ± 0.059	−0.210 ± 0.038	−0.265

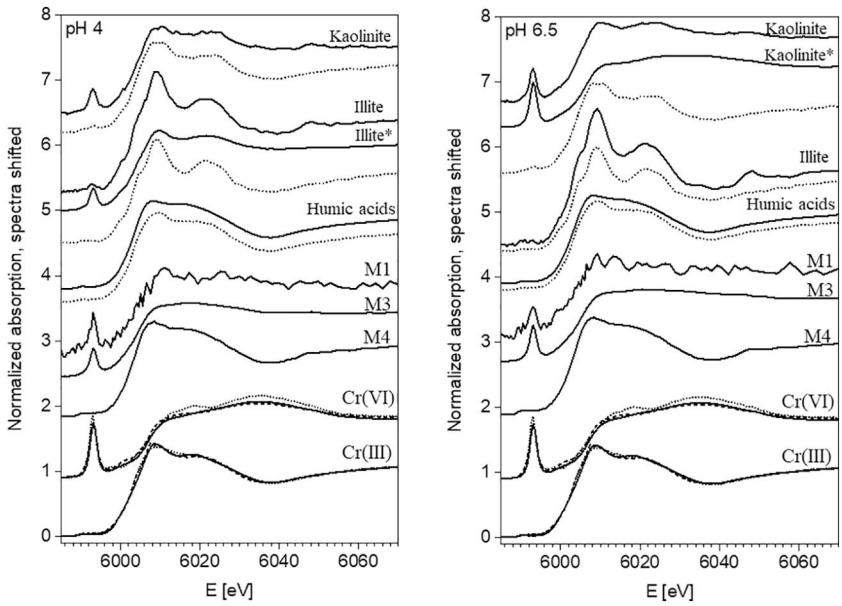

Fig. 2. Cr *K*-XANES spectra for clay minerals, humic acids and mixtures of soil components after Cr(VI) adsorption at pH 4 and 6.5 for initial Cr(VI) concentration of 5×10^{-4} M and spectra of intrinsic Cr of kaolinite, illite and humic acid (dotted lines below the Cr(VI) treated spectra each). Spectra of high- Cr(VI) loaded clay minerals are marked with an asterisk (*). Cr(III) references include $Cr(NO_3)_3$ (solid line), illite (dashed line) and kaolinite (dotted line), both with Cr(VI) reduced by Synchrotron irradiation. Cr(VI) references include Cr(VI) treated ferrihydrite (solid line), $K_2Cr_2O_7$ (dashed line) and $PbCrO_4$ (dotted line). LC-Fit results for each spectrum see in Table 3.

6.5 ($\delta^{53}Cr_{eq(pH4)} = -0.217 \pm 0.081‰$; $\delta^{53}Cr_{eq(pH6.5)} = -0.209 \pm 0.056‰$) (Table 4). In the case of illite, $\delta^{53}Cr_{eq}$ values were close to the $\delta^{53}Cr_{init}$ ($\delta^{53}Cr_{eq(pH4)} = -0.398 \pm 0.004‰$; $\delta^{53}Cr_{eq(pH6.5)} = -0.431 \pm 0.027‰$). Based on the isotopic data, the extent of Cr(VI) reduction seems to be smaller in comparison with XAS results. However, we suppose that $\delta^{53}Cr_{eq}$ values can be, to some extent, affected by the dissolution of intrinsic Cr from kaolinite and illite. The redox-independent Cr isotopic fractionation, induced by dissolution, was already confirmed by Saad et al. (2017). In the case of kaolinite, the effect of potentially dissolved intrinsic Cr(III) ($\delta^{53}Cr = 0.193 \pm 0.040‰$) would be "positive", shifting the $\delta^{53}Cr_{eq}$ towards positive values. In case of illite, the dissolved intrinsic Cr(III) ($\delta^{53}Cr = -0.317 \pm 0.016‰$) would be "negative", shifting the $\delta^{53}Cr_{eq}$ back to more negative values. A more detailed study on the dissolution of Cr(III) originally present within clay minerals is needed in order to evaluate the isotopic data more precisely. On the other hand, a partial adsorption of Cr(VI) onto kaolinite and illite, as confirmed by XAS, was proven to have a negligible effect on Cr isotopic fractionation (Ellis et al., 2004). To verify the isotopic fractionation, the mass balance was applied to isotopic data, considering that Cr(VI) remains in the supernatant after adsorption and Cr(III) is bound to the solid phase (Table S5). In general, the good match between inputs and outputs obtained for both kaolinite and illite is accompanied by some deviations, especially in the case of kaolinite at pH 4 and illite at pH 4 and 6.5. These deviations may be caused both by the adsorption of Cr(VI) from the solution and the desorption of Cr(III) from the clay surfaces.

3.2.3. The ability of humic acids to reduce Cr(VI)

The Cr *K*-edge XANES spectra of humic acids loaded with Cr(VI) confirmed only the presence of reduced Cr(III) at pH 4 as well as at pH 6.5 (Fig. 2). A direct oxidation of humic acids was proven mainly by the formation of either free or dissociated carboxylic groups during Cr (VI) adsorption as observed in FTIR spectra of humic acid at pH 4 and pH 6.5, respectively (Fig. 3). No absorption band is observed at approximately 1540 cm^{-1}, indicating the presence of a chelated carboxylic group due to Cr binding at both pH values (Zhang et al., 2017, 2018). Moreover, no other functional groups able to complex with Cr (VI) were detected on the surface of humic acids (see more in SI). Thus, Cr(VI) is directly reduced (Park et al., 2005; Zhang et al., 2017) in contact with electron donor groups in the aqueous phase under our experimental conditions, and the Cr_2O_3 spectrum of adsorbed Cr(III) can be recognized between 620 and 680 cm^{-1} in both FTIR spectra of humic acids after Cr(VI) treatment.

The reduction of Cr(VI) by humic acids (Hsu et al., 2009; Wittbrodt and Palmer, 1997) is accompanied by an enrichment of heavier Cr isotopes in the supernatant after the adsorption in comparison with the initial Cr solution ($\delta^{53}Cr_{init} = -0.475 \pm 0.020‰$ (2SD, $n = 3$)). The most significant change in the Cr isotopic composition was determined at pH 4 with the maximal relative isotopic difference $\mathbf{\Delta} = 0.5‰$ (Table 4). The $^{53}Cr/^{52}Cr$ shift may reach up to 4‰ depending on the reduction agents (Basu et al., 2014; Ellis et al., 2002; Šillerová et al., 2014). With regard to the character of intrinsic Cr(III) in humic acids as confirmed by XAS, the final Cr isotopic composition in the supernatant after adsorption should not be influenced by intrinsic Cr, thus reflecting Cr(VI) reduction. However, dissolution of humic acids stands in the way of mass balance of humic acids (Table S5). Mass flows cannot be identified well while evaluating the isotopic data for humic acids and due to their solubility over a wide pH range, it is impossible to quantitatively separate the solid and liquid fractions (Melo et al., 2016; Chen et al., 2011). Moreover, dissolution of humic acids constitutes one of the reasons for 2-pK DLM incompatibility with adsorption data for M4.

3.3. Cr(VI) reduction in the mixtures of soil components

Clay minerals should cause Cr(VI) reduction in M1 in the absence of humic acids. LCF of Cr *K*-XANES spectra of M1 indicate 43% and 65% of total Cr in the mixture present as Cr(III) at pH 4 and pH 6.5, respectively (Table 3, Fig. 2). More Cr(VI) adsorbed under acidic conditions could reflect a contribution of inner-sphere monodentate Cr(VI) complexes on kaolinite (Veselská et al., 2016) to inner-sphere Cr(VI) complexes on maghemite. In the presence of maghemite, ferrihydrite and humic acids, the XANES spectra of M3 can be fitted well with the fraction of Cr(VI) adsorbed on ferrihydrite and the fraction of Cr(III) reduced by humic acids (Fig. 2). The decreasing reduction of Cr(VI) with increasing pH (50% and 37% of Cr(III) at pH 4 and 6.5, respectively) reflected strong reduction effect of humic acids, which is more promoted under acidic conditions (Wittbrodt and Palmer, 1996, 1997). In comparison with the Cr *K* XANES spectra for M4 with no ferrihydrite, Cr *K* XANES spectra of M3 show for both pH values significant Cr(VI) fractions. Obviously, ferrihydrite is able to preserve a certain fraction of Cr(VI) even in the presence of humic acids rather than maghemite.

Based on Cr *K*-XANES spectra of M4 (Table 3), Cr(VI) was fitted to an insignificant fraction of < 2%, so that Cr *K*-XANES spectra of M4 could be normalized to the Cr(III) fraction only. Therefore, the major portion of adsorbed Cr(VI) in M4 has been reduced regardless of the pH

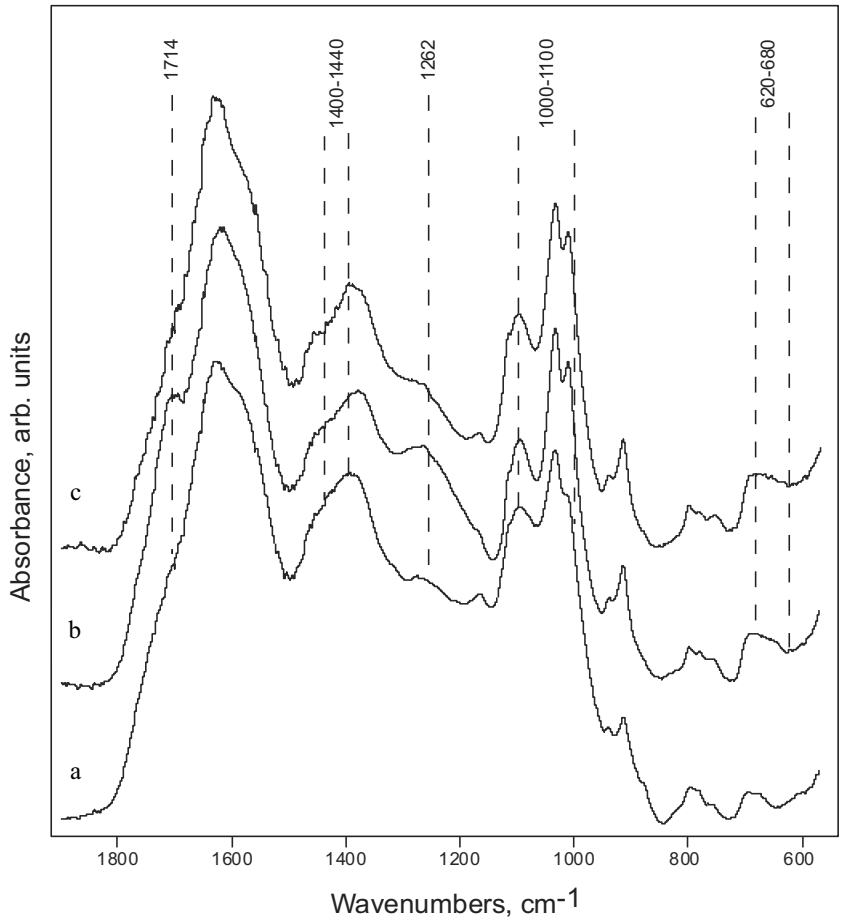

Fig. 3. FTIR spectra of humic acids before (a) and after the Cr(VI) adsorption at pH 4 (b) and pH 6.5 (c).

value (Fig. 2). More than 90% of the Cr(III) fraction can be assigned to humic acids, a small fraction of Cr(III) (7–8%) is bound to illite. In general, Cr(VI) in M4 has been reduced due to the dominant role of humic acids in contrast to M3 where ferrihydrite is present in addition to maghemite. The limited adsorption capacity of other soil components caused by the occupation of their adsorption sites by humic acids also needs to be considered.

4. Conclusions

Our study was based on a multidisciplinary approach investigating the adsorption and reduction of Cr(VI) by synthetic organo-mineral mixtures in the presence or absence of selected soil components (maghemite, ferrihydrite, humic acids) and under specific conditions (pH, ionic strength, Cr(VI) concentration). Based on the results from surface complexation modeling and spectroscopic and isotopic analyses, we evaluated how the soil components affect Cr(VI) behavior in soils. The presence of Fe (oxy)hydroxides increases Cr(VI) removal from solution in a range of pH typical for natural soils, from 5 to 7 (from 70% to 99% of Cr(VI) adsorbed). Fe-rich soils with sandy textures and low organic matter content should be then more susceptible to participate in natural attenuation of Cr(VI), depending on Cr concentration and pH value. Ubiquitous clay minerals support both the adsorption and reduction of Cr(VI) depending mainly on initial Cr(VI) concentration and content of inorganic impurities including TiO_2 and intrinsic Cr. Humic acids adsorb Cr(VI) at pH < 4 likely due to inorganic impurities (Al, Si, Fe, Ca), but the dominant role of the humic acids is through the reduction of Cr(VI) to Cr(III) in the mixtures of soil components over a wide range of Cr(VI) concentrations (from 10^{-6} M to 5×10^{-4} M Cr(VI)) and pH values (3–9).

Despite the large reduction potential of humic acids, ferrihydrite was able to preserve a certain Cr fraction as Cr(VI) in the soil mixtures preventing it from the reduction to Cr(III). On the other hand, the lack of ferrihydrite in natural soils may give rise to the reduction potential of humic acids. This contradiction was manifested more clearly at higher Cr(VI) concentration (up to 5×10^{-4} M). From an environmental risk perspective, soils rich in organic matter and clay minerals will be more efficient at retention of Cr(III) as a product of Cr(VI) reduction. To conclude, a combination of three different approaches has helped to obtain a more comprehensive information about the complex processes of adsorption/reduction of Cr(VI) in soil environments. Results obtained from multiple perspectives can further contribute to elucidate the fate of Cr(VI) in contaminated soils and to develop capable remediation measures.

Acknowledgements

This work was supported by the Czech Science Foundation (grant number 15-17224Y) and Faculty of Agrobiology, Food and Natural Resources, Czech University of Life Sciences Prague (internal project CIGA 20162016). The authors thank to Ondřej Šebek, Radek Fajgar, Roman Skála, Hana Šnajdaufová, Anna Francová, Marie Králová, Filip Šmat and Jahongir Rustamov for help with isotopic and spectroscopic analyses, X-ray diffraction and laboratory experiments. The authors thank three anonymous reviewers for their constructive comments and suggestions.

Appendix A. Supplementary data

Supplementary data to this article can be found online at https://doi.org/10.1016/j.envint.2019.03.066.

References

Ahmed, M.A., Elsir, A.T., Mohammed, F., Elbushra, H.A., Tawer, S., Eassa, N., 2018. Photo-reduction of chromium from water by TiO_2 nanoparticles. Afri. Mater. Res. Soc. 3, 2667–2674.

Ajouyed, O., Hurel, C., Marmier, N., 2011. Evaluation of the adsorption of hexavalent chromium on kaolinite and illite. J. Environ. Prot. 2, 1347–1352.

Al-Essa, K., Khalili, F., 2018. Adsorption of humic acid onto Jordanian kaolinite clay: effects of humic acid concentration, pH, and temperature. Sci. J. Chem. 6 (1), 10.

Basu, A., Johnson, T.M., 2012. Determination of hexavalent chromium reduction using Cr stable isotopes: isotopic fractionation factors for permeable reactive barrier materials. Environ. Sci. Technol. 46, 5353–5360.

Basu, A., Johnson, T.M., Sanford, R.A., 2014. Cr isotope fractionation factors for Cr(VI) reduction by a metabolically diverse group of bacteria. Geochim. Cosmochim. Acta 142, 349–361.

Bauer, K.W., Gueguen, B., Cole, D.B., Francois, R., Kallmeyer, J., Planavsky, N., Crowe, S.A., 2018. Chromium isotope fractionation in ferruginous sediments. Geochim. Cosmochim. Acta 223, 198–215.

Blowes, D., 2002. Tracking hexavalent Cr in groundwater. Science 295, 2024–2025.

Borisover, M., Davis, J.A., 2015. Adsorption of inorganic and organic solutes by clay minerals, 2015. Dev. Clay Sci. 6, 33–70.

Bullen, T.D., 2007. Chromium stable isotopes as a new tool for forensic hydrology at sites contaminated with anthropogenic chromium. In: Bullen, T.D., Wang, Y. (Eds.), Water-rock Interaction, Proceedings and Monographs in Engineering, Water and Earth Sciences, pp. 699–702.

Chen, S.Y., Huang, S.W., Chiang, P.N., Liu, J.C., Kuan, W.H., Huang, J.H., Hung, J.T., Tzou, Y.M., Chen, C.C., Wang, M.K., 2011. Influence of chemical compositions and molecular weights of humic acids on Cr (VI) photo-reduction. J. Hazard. Mater. 197, 337–344.

Chen, H., Koopal, L., Xiong, J., Avena, M., Tan, W., 2017. Mechanisms of soil humic acid adsorption onto montmorillonite and kaolinite. J. Colloid Interface Sci. 504 (457-46).

Dinker, M.K., Kulkarni, P.S., 2015. Recent advances in silica-based materials for the removal of hexavalent chromium: a review. J. Chem. Eng. Data 60, 2521–2540.

Economou-Eliopoulos, M., Frei, R., Atsarou, C., 2014. Application of chromium stable isotopes to the evaluation of Cr(VI) contamination in groundwater and rock leachates from central Euboea and the Assopos basin (Greece). Catena 122, 216–228.

Ellis, A.S., Johnson, T.M., Bullen, T.D., 2002. Chromium isotopes and the fate of hexavalent chromium in the environment. Science 295, 2060–2062.

Ellis, A.S., Johnson, T.M., Bullen, T.D., 2004. Using chromium stable isotopes to quantify Cr(VI) reduction: lack of sorption effect. Environ. Sci. Technol. 38, 3604–3607.

Farkaš, J., Chrastný, V., Novák, M., Čadková, E., Pašava, J., Chakrabarti, R., Jacobsen, S.B., Ackerman, L., Bullen, T.D., 2013. Chromium isotope variations ($\delta^{53/52}$Cr) in mantle-derived sources and their weathering products: implications for environmental studies and the evolution of $\delta^{53/52}$Cr in the Earth's mantle over geologic time. Geochim. Cosmochim. Acta 123, 74–92.

Ginder-Vogel, M., Sparks, D.L., 2010. The impacts of X-ray absorption spectroscopy on understanding soil processes and reaction mechanisms. In: Balwant, S., Markus, G. (Eds.), Developments in Soil Science, Elsevier, 2010, 2014, pp. 1–26 (Chapter 1).

Gu, X., Xie, J., Wang, X., Evans, L.J., 2017. A simple model to predict chromate partitioning in selected soils from China. J. Hazard. Mater. 322, 421–429.

Gunkel-Grillon, P., Laporte-Magoni, C., Lemestre, M., Bazire, N., 2014. Toxic chromium release from nickel mining sediments in surface waters, New Caledonia. Environ. Chem. Lett. 12, 511–516.

Gustafsson, J.P., 2009. Modelling metal sorption in soils. In: Modelling of Pollutants in Complex Environmental Systems. 1. pp. 145–176.

Gustafsson, J.P., 2013. Visual MINTEQ. Version 3.1. Division of Land and Water Resources. Royal Institute of Technology, Stockholm, Sweden.

Hausladen, D.M., Fendorf, S., 2017. Hexavalent chromium generation within naturally structured soils and sediments. Environ. Sci. Technol. 51, 2058–2067.

He, Z., Cai, Q., Wu, M., Shi, Y., Fang, H., Li, L., Chen, J., Chen, J., Song, S., 2013. Photocatalytic reduction of Cr(VI) in an aqueous suspension of surface-fluorinated anatase TiO_2 nanosheets with exposed {001} facets. Ind. Eng. Chem. Res. 52, 9556–9565.

Herbelin, A.L., Westall, J.C., 1999. FITEQL 4.0: A Computer Program for Determination of Chemical Equilibrium Constants from Experimental Data; Report 99-01. Department of Chemistry, Oregon State University, Corvallis.

Hopp, L., Nico, P.S., Marcus, M.A., Peiffer, S., 2008. Arsenic and chromium partitioning in a podzolic soil contaminated by chromated copper arsenate. Environ. Sci. Technol. 42, 6481–6486.

Hori, M., Shozugawa, K., Matsuo, M., 2015. Reduction process of Cr(VI) by Fe(II) and humic acid analyzed using high time resolution XAFS analysis. J. Hazard. Mater. 285, 140–147.

Hsu, N.H., Wang, S.L., Lin, Y.C., Sheng, G.D., Lee, J.F., 2009. Reduction of Cr(VI) by crop-residue-derived black carbon. Environ. Sci. Technol. 43, 8801–8806.

Hsu, L.C., Liu, Y.T., Tzou, Y.M., 2015. Comparison of the spectroscopic speciation and chemical fractionation of chromium in contaminated paddy soils. J. Hazard. Mater. 296, 230–238.

Izbicki, J.A., Ball, J.W., Bullen, T.D., Sutley, S.J., 2008. Chromium, chromium isotopes and selected trace elements, Western Mojave Desert, USA. Appl. Geochem. 23, 1325–1352.

Jamieson-Hanes, J.H., Amos, R.T., Blowes, D.W., Ptacek, C.J., 2015. Dual mechanism conceptual model for Cr isotope fractionation during reduction by zerovalent iron under saturated flow conditions. Environ. Sci. Technol. 49, 5467–5475.

Jardine, P.M., Stewart, M.A., Barnett, M.O., Basta, N.T., Brooks, S.C., Fendorf, S., Mehlhorn, T.L., 2013. Influence of soil geochemical and physical properties on chromium(VI) sorption and bioaccessibility. Environ. Sci. Technol. 47, 11241–11248.

Jiang, W., Cai, Q., Xu, W., Yang, M., Cai, Y., Dionysiou, D.D., O'Shea, K.E., 2014. Cr(VI) adsorption and reduction by humic acid coated on magnetite. Environ. Sci. Technol. 48, 8078–8085.

Jin, W., Du, H., Zheng, S., Zhang, Y., 2016. Electrochemical processes for the environmental remediation of toxic Cr(VI): a review. Electrochim. Acta 191, 1044–1055.

Joe-Wong, C., Brown, G.E., Maher, K., 2017. Kinetics and products of chromium(VI) reduction by iron(II/III)-bearing clay minerals. Environ. Sci. Technol. 51, 9817–9825.

Johnston, C.P., Chrysochoou, M., 2016. Mechanisms of chromate, selenate, and sulfate adsorption on Al-substituted ferrihydrite: implications for ferrihydrite surface structure and reactivity. Environ. Sci. Technol. 50, 3589–3596.

Jolsterå, R., Gunneriusson, L., Forsling, W., 2010. Adsorption and surface complex modeling of silicates on maghemite in aqueous suspensions. J. Colloid Interface Sci. 342, 493–498.

Kamagaté, M., Lützenkirchen, J., Huber, F., Hanna, K., 2016. Comment on "Competitive adsorption of Cd(II), Cr(VI), and Pb(II) onto nanomaghemite: a spectroscopic and modeling approach". Environ. Sci. Technol. 50, 1632–1633.

Kitchen, J.W., Johnson, T.M., Bullen, T.D., Zhu, J., Raddatz, A., 2012. Chromium isotope fractionation factors for reduction of Cr(VI) by aqueous Fe(II) and organic molecules. Geochim. Cosmochim. Acta 89, 190–201.

Komárek, M., Koretsky, C.M., Stephen, K.J., Allesi, D.S., Chrastný, V., 2015. Competitive adsorption of cd(II), Cr(VI), and Pb(II) onto nanomaghemite: a spectroscopic and modeling approach. Environ. Sci. Technol. 49, 12851–12859.

Koretsky, C., 2000. The significance of surface complexation reactions in hydrologic systems: a geochemist's perspective. J. Hydrol. 230, 127–171.

Koretsky, C.M., 2013. Development of surface complexation models of Cr(VI) adsorption on soils, sediments and model mixtures of kaolinite, montmorillonite, γ-alumina, hydrous manganese and ferric oxides and goethite. In: Technical Report. Western Michigan University, United States.

Kožuh, N., Štupar, J., Gorenc, B., 2000. Reduction and oxidation processes of chromium in soils. Environ. Sci. Technol. 34, 112–119.

Kwak, S., Yoo, J.C., Moon, D.K., Baek, K., 2018. Role of clay minerals on reduction of Cr (VI). Geoderma 312, 1–5.

Li, D., Ji, G., Hu, J., Hu, S., Yuan, X., 2018. Remediation strategy and electrochemistry flushing & reduction technology for real Cr (VI)-contaminated soils. Chem. Eng. J. 334, 1281–1288.

McDermott, S., Salzberg, D.C., Anderson, A.P., Shaw, T., Lead, J., 2015. Systematic review of chromium and nickel exposure during pregnancy and impact on child outcomes. J. Toxicol. Environ. Health, Part A 78, 1348–1368.

Melo, B.A.G., Motta, F.L., Santana, M.H.A., 2016. Humic acids: structural and multiple functionalities for novel technological developments. Mater. Sci. Eng. C 62, 967–974.

Mishra, S., Bharagava, R.N., 2016. Toxic and genotoxic effects of hexavalent chromium in environment and its bioremediation strategies. J. Environ. Sci. Health C Environ. Carcinog. Ecotoxicol. Rev. 34, 1–32.

Mollon, L.C., Norton, G.J., Trakal, L., Moreno-Jimenez, E., Elouali, F.Z., Hough, R.L., Beesley, L., 2016. Mobility and toxicity of heavy metal(loid)s arising from contaminated wood ash application to a pasture grassland soil. Environ. Pollut. 218, 419–427.

Novak, M., Chrastny, V., Cadkova, E., Farkas, J., Bullen, T.D., Tylcer, J., Szurmanova, Z., Cron, M., Prechova, E., Curik, J., Stepanova, M., Pasava, J., Erbanova, L., Houskova, M., Puncochar, K., Hellerich, L.A., 2014. Common occurrence of a positive δ53Cr shift in central European waters contaminated by geogenic/industrial chromium relative to source values. Environ. Sci. Technol. 48, 6089–6096.

Novak, M., Kram, P., Sebek, O., Andronikov, A., Chrastny, V., Martinkova, E., Stepanova, M., Prechova, E., Curik, J., Veselovsky, F., Myska, O., Stedra, V., Farkas, J., 2017. Temporal changes in Cr fluxes and δ^{53}Cr values in runoff from a small serpentinite catchment (Slavkov Forest, Czech Republic). Chem. Geol. 472, 22–30.

Novak, M., Sebek, O., Chrastny, V., Hellerich, L.A., Andronikov, A., Martinkova, E., Farkas, J., Pacherova, P., Curik, J., Stepanova, M., Prechova, E., Houskova, M., Zoulova, V., Veselovsky, F., Svobodova, I., Janotova, P., Komarek, A., 2018. Comparison of $\delta^{53}Cr_{Cr(VI)}$ values of contaminated groundwater at two industrial sites in the eastern U.S. with contrasting availability of reducing agents. Chem. Geol. 481, 74–84.

Park, D., Yun, Y.S., Jo, J.H., Park, J.M., 2005. Mechanism of hexavalent chromium removal by dead fungal biomass of *Aspergillus niger*. Water Res. 39, 533–540.

Pérez, C., Antelo, J., Fiol, S., Arce, F., 2014. Modeling oxyanion adsorption on ferralic soil, part 2: chromate, selenate, molybdenate, and arsenate adsorption. Environ. Toxicol. Chem. 33, 2217–2224.

Peterson, M.L., Brown Jr., G.E., Parks, G.A., 1996. Direct XAFS evidence for heterogeneous redox reaction at the aqueous chromium/magnetite interface. Colloids Surf. A Physicochem. Eng. Asp. 107, 77–88.

Pradhan, D., Sukla, L.B., Sawyer, M., Rahman, P.K.S.M., 2017. Recent bioreduction of hexavalent chromium in wastewater treatment: a review. J. Ind. Eng. Chem. 55, 1–20.

Quin, L., Wang, X., 2017. Chromium isotope geochemistry. Rev. Mineral. Geochem. 82, 379–408.

Ravel, B., Newville, M., 2005. ATHENA, ARTEMIS, HEPHAESTUS: data analysis for X-ray absorption spectroscopy using IFEFFIT. J. Synchrotron Radiat. 12, 537–541.

Reich, T.J., Koretsky, C.M., 2011. Adsorption of Cr(VI) on γ-alumina in the presence and absence of CO_2: comparison of three surface complexation models. Geochim.

Cosmochim. Acta 75, 7006–7017.
Rinehart, T.L., Schulze, D.G., Bricka, R.M., Bajt, S., Blatchley, E.R., 1997. Chromium leaching vs. oxidation state for a contaminated solidified/stabilized soil. J. Hazard. Mater. 52, 213–221.
Saad, E.M., Wang, X., Planavsky, N.J., Reinhard, C.T., Tang, Y., 2017. Redox-independent chromium isotope fractionation induced by ligand-promoted dissolution. Nat. Commun. 8, 1590.
Schwertmann, U., Cornell, R.M., 2000. Iron Oxides in the Laboratory: Preparation and Characterization, second ed. Wiley-VCH Verlag GmbH, Weinheim.
Shadid, M., Shamshad, S., Rafiq, M., Khalid, S., Bibi, I., Niazi, N.K., Dumat, C., Rashid, M.I., 2017. Chromium speciation, bioavailability, uptake, toxicity and detoxification in soil-plant system: a review. Chemosphere 178, 513–533.
Šillerová, H., Chrastný, V., Čadková, E., Komárek, M., 2014. Isotope fractionation and spectroscopic analysis as an evidence of Cr(VI) reduction during biosorption. Chemosphere 95, 402–407.
Stucki, J.W., 2013. Properties and behaviour of iron in clay minerals. In: Developments in Clay Science. vol. 5A. Elsevier, pp. 559–611.
Taylor, R.W., Shen, S., Bleam, W.F., Tu, S.I., 2000. Chromate removal by dithionite-reduced clays: evidence from direct X-ray adsorption near edge spectroscopy (XANES) of chromate reduction at clay surfaces. Clay Clay Miner. 48, 648–654.
Turner, B.F., Fein, J.B., 2006. Protofit: a program for determining surface protonation constants from titration data. Comput. Geosci. 32, 1344–1356.
Veselská, V., Fajgar, R., Číhalová, S., Bolanz, R.M., Göttlicher, J., Steininger, R., Siddique, J.A., Komárek, M., 2016. Chromate adsorption on selected soil minerals: surface complexation modeling coupled with spectroscopic investigation. J. Hazard. Mater. 318, 433–442.
Vinuth, M., Naik, H.S.B., Manjanna, J., Vinoda, B.M., 2015. Environmental remediation of hexavalent chromium in aqueous medium using Fe (II)-montmorillonite as reductant. Prog Earth Planet Sci 11, 275–283.
Wanner, C., Zink, S., Eggenberger, U., Mäder, U., 2012. Assessing the Cr(VI) reduction efficiency of a permeable reactive barrier using Cr isotope measurements and 2D reactive transport modeling. J. Contam. Hydrol. 131, 54–63.
Wittbrodt, P.R., Palmer, C.D., 1996. Effect of temperature, ionic strength, background electrolytes, and Fe(III) on the reduction of hexavalent chromium by soil humic substances. Environ. Sci. Technol. 30, 2470–2477.
Wittbrodt, P.R., Palmer, C.D., 1997. Reduction of Cr(VI) by soil humic acids. Eur. J. Soil Sci. 48, 151–162.
Wu, J., Zhang, J., Xiao, C., 2016. Focus on factors affecting pH, flow of Cr and transformation between Cr (VI) and Cr (III) in the soil with different electrolytes. Electrochim. Acta 211, 652–662.
Xie, J., Gu, X., Tong, F., Zhao, Y., Tan, Y., 2015. Surface complexation modeling of Cr (VI) adsorption at the goethite–water interface. J. Colloid Interface Sci. 455, 55–62.
Xu, F., Ma, T., Zhou, L., Hu, Z., Shi, L., 2015. Chromium isotopic fractionation during Cr (VI) reduction by *Bacillus* sp. under aerobic conditions. Chemosphere 130, 46–51.
Zhang, J., Chen, L., Yin, H., Jin, S., Liu, F., Chen, H., 2017. Mechanism study of humic acid functional groups for Cr(VI) retention: two-dimensional FTIR and ^{13}C CP/MAS NMR correlation spectroscopic analysis. Environ. Pollut. 225, 86–92.
Zhang, J., Yin, H., Chen, L., Liu, F., Chen, H., 2018. The role of different functional groups in a novel adsorption-complexation-reduction multi-step kinetic model for hexavalent chromium retention by undissolved humic acid. Environ. Pollut. 237, 740–746.
Zink, S., Schoenberg, R., Staubwasser, M., 2010. Isotopic fractionation and reaction kinetics between Cr(III) and Cr(VI) in aqueous media. Geochim. Cosmochim. Acta 74, 5729–5745.